

# Theory of infrared magneto-optical effects from chiral phonons in solids

Chiara Fiorazzo,<sup>1,\*</sup> Cheol-Hwan Park,<sup>2,3,4,5,†</sup> Ivo Souza,<sup>4,6,‡</sup> and Matteo Calandra<sup>1,§</sup>

<sup>1</sup>*Department of Physics, University of Trento, Via Sommarive 14, 38123 Povo, Italy*

<sup>2</sup>*Department of Physics and Astronomy, Seoul National University, Seoul 08826, Korea*

<sup>3</sup>*Center for Theoretical Physics, Seoul National University, Seoul 08826, Korea*

<sup>4</sup>*Centro de Física de Materiales, Universidad del País Vasco, 20018 San Sebastián, Spain*

<sup>5</sup>*Donostia International Physics Center, 20018 San Sebastián, Spain*

<sup>6</sup>*Ikerbasque Foundation, 48013 Bilbao, Spain*

(Dated: June 16, 2025)

In crystals with broken time-reversal symmetry, zone-center phonons can acquire a finite angular momentum via velocity-dependent forces on the nuclei. Despite having the same order of magnitude as the electron spin angular momentum, the phonon angular momentum can be hard to detect because the frequency splitting is small. Here, by developing a theory of lattice magneto-optical effects in reflection and transmission, we show that infrared magnetic circular dichroism is a sensitive probe of zone-center phonon chirality. We evaluate the infrared magneto-optical Faraday, Kerr, and circular-dichroism spectra of CrI<sub>3</sub> from time-dependent density-functional theory in the adiabatic local-density approximation. We find sizeable circular dichroism from the infrared-active E<sub>u</sub> mode at  $\approx 214$  cm<sup>-1</sup>, even though the calculated splitting is only 0.22 cm<sup>-1</sup>.

## I. INTRODUCTION

The observation of the phonon Hall effect in 2005 [1] brought renewed attention to the subtle coupling of lattice vibrations to external magnetic fields [2, 3] and, by extension, to internal magnetic order [4–7]. Lattice vibrations are typically treated in the Born-Oppenheimer approximation [8], where the only (harmonic) coupling to electrons is via the interatomic force-constant (IFC) matrix. Since the IFC is a static response function, any time-reversal breaking that may be present in the electronic wave functions is not transmitted to the lattice degrees of freedom. As a result, phonon Hall and other effects arising from broken time-reversal phonons are absent from that description; in particular, nondegenerate zone-center phonon modes are linearly polarized (away from  $\Gamma$  they can become elliptically polarized if inversion symmetry is broken, leading to observable effects [9, 10]).

Once time-reversal is broken in the lattice dynamics, degenerate linearly-polarized phonon modes at  $\Gamma$  may split into nondegenerate elliptically-polarized (“chiral”) modes carrying a net angular momentum [5]. To capture such effect, one must go beyond the static approximation in the description of interatomic forces. In the Born-Oppenheimer scheme, this is achieved by including the nuclear geometric vector potential [2, 11], which gives rise to velocity-dependent forces mediated by the nuclear Berry curvature [3, 6]. Alternatively, one may start from a nonadiabatic (dynamical) electron-phonon response function; the “velocity-force” coupling is then recovered by expanding the dynamical IFC matrix to first order in frequency [12].

Recently, chiral vibration modes induced by velocity-dependent forces have been studied from first principles in magnetic molecules [12] and solids [13, 14]. These works highlighted the role of relativistic effects and non-collinear magnetism in the generation of a net vibrational angular momentum. Experimental detection of this effect is a challenging task; the main difficulty is that the frequency splittings are small, of the order of 1 cm<sup>-1</sup> or less, even when the phonon angular momentum is of the order of  $\hbar/2$ . Nevertheless, the chirality of Raman-active zone-center phonons in magnetic crystals has been detected by the reversal of helicity of circularly-polarized incident light [15, 16], and possible signatures in infrared (IR) spectroscopy have also been suggested [12, 14].

In this work, we propose IR magneto-optical effects as sensitive probes of mode-resolved zone-center phonon angular momentum. Quite generally, magneto-optical effects in the electric-dipole approximation (Faraday and Kerr rotation, magnetic circular dichroism [17]) are sensitive to a net (macroscopic) magnetization. They are associated with the presence of a nonzero antisymmetric (AS) part in the dielectric function,

$$\epsilon_{\alpha\beta}^{\text{AS}}(\omega) = \frac{\epsilon_{\alpha\beta}(\omega) - \epsilon_{\beta\alpha}(\omega)}{2}, \quad (1)$$

which is time-odd according to the Onsager relation. Working in the framework of time-dependent density-functional theory (TDDFT), we evaluate the lattice-mediated contribution to Eq. (1) in the adiabatic local density approximation and find that it is induced by the nuclear Berry curvature. In addition, we obtain expressions for the magnetic circular dichroic absorbance and for the Faraday and Kerr rotation strengths, taking into account the sample thickness for effects in transmission. We apply our formalism to bulk CrI<sub>3</sub> and show that the predicted circular dichroism is sizeable, suggesting that it can be used to detect the phonon angular momentum of IR-active modes.

\* chiara.fiorazzo@unitn.it

† cheolhwan@snu.ac.kr

‡ ivo.souza@ehu.es

§ m.calandrabuonaura@unitn.it

The paper is organized as follows. In Sec. II we develop the non-adiabatic linear response theory leading to the antisymmetric part of the dynamic infrared dielectric function. In Sec. III we explain the technical details of the first principles time dependent density functional theory calculation. In sec. IV we apply the theory and the methodological developments to the circular dichroic absorption and to the Faraday and Kerr effects in CrI<sub>3</sub>. Finally we draw the conclusions.

## II. THEORY

### A. Definitions

We consider a crystal composed of  $N$  cells under periodic boundary conditions, and with  $N_a$  atoms in the unit cell. The position of an atom is identified by the vector

$$\mathbf{R}_{La} \equiv \mathbf{R}_L + \boldsymbol{\tau}_a + \mathbf{u}_{La}, \quad (2)$$

where  $\mathbf{R}_L$  is a direct lattice vector,  $\boldsymbol{\tau}_a$  the equilibrium position of the  $a$ -th atom in the unit cell, and  $\mathbf{u}_{La}$  indicates the deviation from equilibrium of the nuclear position. The equilibrium positions are determined by the condition of vanishing forces, i.e.

$$\mathbf{F}_{La} = - \left. \frac{\partial E(\mathbf{R})}{\partial \mathbf{R}_{La}} \right|_{\mathbf{u}=\mathbf{0}} = \mathbf{0}, \quad (3)$$

where  $E(\mathbf{R})$  is the Born-Oppenheimer energy surface.

We introduce the adiabatic force-constant matrix

$$C_{a\alpha, b\beta}(\mathbf{R}_L - \mathbf{R}_M) = \left. \frac{\partial^2 E(\mathbf{R})}{\partial R_{La\alpha} \partial R_{Mb\beta}} \right|_{\mathbf{u}=\mathbf{0}}, \quad (4)$$

where  $\alpha$  and  $\beta$  are Cartesian indices.

We define the Fourier transform of the atomic displacement from equilibrium as

$$\mathbf{u}_{\mathbf{q}a} = \frac{1}{N} \sum_L \mathbf{u}_{La} e^{-i\mathbf{q}\cdot\mathbf{R}_L}, \quad (5)$$

and similarly,

$$C_{a\alpha, b\beta}(\mathbf{q}) = \frac{1}{N} \frac{\partial^2 E(\mathbf{R})}{\partial u_{\mathbf{q}a\alpha}^* \partial u_{\mathbf{q}b\beta}}. \quad (6)$$

The dynamical matrix in Fourier space is obtained by dividing the force constant matrix by the square root of the masses of the atoms. In the adiabatic approximation we find

$$D_{a\alpha, b\beta}(\mathbf{q}) = \frac{C_{a\alpha, b\beta}(\mathbf{q})}{\sqrt{M_a} \sqrt{M_b}}. \quad (7)$$

The diagonalization of the adiabatic dynamical matrix in Fourier space leads to the adiabatic phonon frequencies  $\omega_{\mathbf{q}\nu}$  and eigenvectors  $\mathbf{e}_{\mathbf{q}\nu}$ , namely

$$\sum_{b\beta} [D_{a\alpha, b\beta}(\mathbf{q}) - \omega_{\mathbf{q}\nu}^2 \delta_{ab} \delta_{\alpha\beta}] e_{\mathbf{q}\nu}^{b\beta} = 0 \quad (8)$$

where  $e_{\mathbf{q}\nu}^{b\beta} = \sqrt{M_b} u_{\mathbf{q}\nu}^{b\beta}$  are the Cartesian components of the phonon eigenvectors. We assume the eigenvectors to be normalized to unity. The adiabatic phonon eigenvectors at the zone center can be taken as yielding linearly-polarized (nonchiral) phonons, and a symmetric (time-even) lattice dielectric function.

### B. Nonadiabatic dielectric function

An infrared oscillating external electric field acts on an insulating crystal of gap  $\Delta$  at  $t = 0$ . More specifically, we consider a monochromatic oscillating electric field of the form

$$\mathcal{E}_\alpha(t) = \mathcal{E}_\alpha e^{-i\omega t} + \text{c.c.} \quad (9)$$

where ‘‘c.c.’’ stands for complex conjugate and  $\omega < \Delta$ . The electric field induces a monochromatic displacement in the ions. As a result,

$$\mathbf{u}_{La}(t) = \mathbf{u}_{La} e^{-i\omega t} + \text{c.c.} \quad (10)$$

In order to obtain the equations of motion of the ions under the action of the oscillating field, we need to calculate the time-dependent retarded force constant matrix, namely

$$C_{a\alpha, b\beta}(\mathbf{q}, t - t') = \frac{1}{N} \frac{\partial^2 E(\mathbf{R})}{\partial u_{\mathbf{q}a\alpha}^*(t') \partial u_{\mathbf{q}b\beta}(t)} \theta(t - t') \quad (11)$$

where  $\theta(t - t')$  is the Heaviside function enforcing the retarded character of the response.

The  $\omega$ -transform of the force constant matrix reads

$$C_{a\alpha, b\beta}(\mathbf{q}, \omega) = \int dt C_{a\alpha, b\beta}(\mathbf{q}, t) e^{i\omega t} \quad (12)$$

The equation of motion for the Fourier transform of the ionic displacement at the zone center ( $\mathbf{q} = \mathbf{0}$ ) reads:

$$M_a \omega^2 u_{\mathbf{0}a\alpha} = \sum_{b\beta} C_{a\alpha, b\beta}(\omega) u_{\mathbf{0}b\beta} - i\hbar\omega \Gamma_a u_{\mathbf{0}a\alpha} - \sum_{\beta} Z_{a\beta\alpha}^* \mathcal{E}_\beta. \quad (13)$$

In this expression  $C_{a\alpha,b\beta}(\omega)$  denotes  $C_{a\alpha,b\beta}(\mathbf{0},\omega)$ , and  $Z_{a\beta\alpha}^*$  is the Born effective charge tensor.  $\Gamma_a$  is the drag-force coefficient for atom  $a$ , and  $u_{\mathbf{0}a\alpha}$  is the Fourier transform of the coefficient  $u_{La\alpha}$  on the right-hand side of Eq. (10).

Within time dependent density functional theory and

in the adiabatic local density approximation, the non-adiabatic force constant matrix for frequencies  $\omega$  smaller than the single-particle gap  $\Delta$  has the form [18]

$$C_{a\alpha,b\beta}(\omega) \approx C_{a\alpha,b\beta}(\omega = 0) + \Pi_{a\alpha,b\beta}(\omega), \quad (14)$$

with

$$\Pi_{a\alpha,b\beta}(\omega) = \frac{1}{N} \sum_{\mathbf{k}} \sum_{mn} \left[ \frac{f_{\mathbf{k}m} - f_{\mathbf{k}n}}{E_{\mathbf{k}m} - E_{\mathbf{k}n} + \hbar\omega} - \frac{f_{\mathbf{k}m} - f_{\mathbf{k}n}}{E_{\mathbf{k}m} - E_{\mathbf{k}n}} \right] \left\langle u_{\mathbf{k}n} \left| \frac{\partial H_{\text{KS}}}{\partial u_{\mathbf{0}a\alpha}} \right| u_{\mathbf{k}m} \right\rangle \left\langle u_{\mathbf{k}m} \left| \frac{\partial H_{\text{KS}}}{\partial u_{\mathbf{0}b\beta}} \right| u_{\mathbf{k}n} \right\rangle. \quad (15)$$

Here  $H_{\text{KS}}$  is the static Kohn-Sham Hamiltonian in the absence of the electric field,  $E_{\mathbf{k}n}$  and  $E_{\mathbf{k}m}$  are the Kohn-Sham single-particle energies,  $f_{\mathbf{k}n}$  is the Fermi function, and  $u_{\mathbf{k}n}$  is the cell-periodic part of the Bloch function.

By substituting Eqs. (14) and (15) into the equations of motions and solving for the Cartesian components of the  $\mathbf{q} = \mathbf{0}$  phonon eigenvector  $e_{\mathbf{0}\alpha}^{a\alpha}$ , we obtain

$$e_{\mathbf{0}\alpha}^{a\alpha} = \sum_{b\beta\gamma} \left[ D(\omega) - \omega^2 - i\omega\tilde{\Gamma} \right]_{a\alpha,b\beta}^{-1} \frac{Z_{b\gamma\beta}^* \mathcal{E}_\gamma}{\sqrt{M_b}} \quad (16)$$

where we have defined  $\tilde{\Gamma}_{a\alpha,b\gamma} = \frac{\Gamma_a}{M_a} \delta_{ab} \delta_{\alpha\gamma}$  and

$$D_{a\alpha,b\beta}(\omega) = \frac{C_{a\alpha,b\beta}(\omega)}{\sqrt{M_a}\sqrt{M_b}}. \quad (17)$$

The  $\alpha$  component of the electric polarization induced by the optical electric field is given by:

$$P_\alpha = \sum_{\beta} \chi_{\alpha\beta}^{\text{el}} \mathcal{E}_\beta + \frac{1}{V_0} \sum_{a\beta} Z_{a\alpha\beta}^* u_{\mathbf{0}a\beta} \equiv \sum_{\beta} \chi_{\alpha\beta} \mathcal{E}_\beta, \quad (18)$$

with  $\chi_{\alpha\beta}^{\text{el}}$  the electronic (clamped-ion) susceptibility and  $V_0$  the unit-cell volume. It follows that the dielectric tensor reads

$$\epsilon_{\alpha\beta}(\omega) = \epsilon_{\alpha\beta}^\infty + \frac{4\pi}{V_0} \sum_{ab} \sum_{\gamma\eta} \frac{Z_{a\alpha\gamma}^*}{\sqrt{M_a}} \left[ D(\omega) - \omega^2 - i\omega\tilde{\Gamma} \right]_{a\gamma,b\eta}^{-1} \frac{Z_{b\beta\eta}^*}{\sqrt{M_b}}, \quad (19)$$

where  $\epsilon_{\alpha\beta}^\infty = 1 + 4\pi\chi_{\alpha\beta}^{\text{el}}$ . We now define the adiabatic mode effective charge for the phonon band  $\nu$  at the zone center as

$$Z_{\nu\alpha}^* = \sum_{a\beta} Z_{a\alpha\beta}^* \frac{e_{\mathbf{0}\nu}^{a\beta}}{\sqrt{M_a}}. \quad (20)$$

As the adiabatic zone-center phonon eigenvectors  $e_{\mathbf{0}\nu}^{a\beta}$  can be chosen as real,  $Z_{\nu\alpha}^*$  is also a real quantity.

We can then write the inner product in the dielectric function by transforming it in the normal-mode basis,

$$\epsilon_{\alpha\beta}(\omega) = \epsilon_{\alpha\beta}^\infty + \frac{4\pi}{V_0} \sum_{\mu\nu} Z_{\mu\alpha}^* \left[ D(\omega) - \omega^2 - i\omega\Gamma^0 \right]_{\mu\nu}^{-1} Z_{\nu\beta}^* \quad (21)$$

where  $\Gamma_{\mu\nu}^0 = \sum_{a\alpha} \frac{e_{\mathbf{0}\mu}^{a\alpha} \Gamma_a e_{\mathbf{0}\nu}^{a\alpha}}{M_a}$ .

The nonadiabatic dynamical matrix can be expressed via Eq. (14) in the normal-mode basis as

$$D_{\mu\nu}(\omega) \approx D_{\mu\nu}(\omega = 0) + \bar{\Pi}_{\mu\nu}(\omega), \quad (22)$$

where  $D_{\mu\nu}(\omega = 0)$  is the adiabatic dynamical matrix introduced earlier, which is diagonal on the basis of the adiabatic eigenmodes, while the nonadiabatic [18] correction reads

$$\bar{\Pi}_{\mu\nu}(\omega) = \frac{1}{N} \sum_{\mathbf{k}} \sum_{n,m} \left[ \frac{f_{\mathbf{k}m} - f_{\mathbf{k}n}}{E_{\mathbf{k}m} - E_{\mathbf{k}n} + \hbar\omega} - \frac{f_{\mathbf{k}m} - f_{\mathbf{k}n}}{E_{\mathbf{k}m} - E_{\mathbf{k}n}} \right] \left\langle u_{\mathbf{k}n} \left| \frac{\partial H_{\text{KS}}}{\partial \mathbf{e}_{\mathbf{0}\mu}} \right| u_{\mathbf{k}m} \right\rangle \left\langle u_{\mathbf{k}m} \left| \frac{\partial H_{\text{KS}}}{\partial \mathbf{e}_{\mathbf{0}\nu}} \right| u_{\mathbf{k}n} \right\rangle. \quad (23)$$

It is worthwhile underlying that Eq. 21 is the nonadiabatic version of Eq. (50) in Ref. [19].

The antisymmetric part of the dielectric function is obtained from Eq. (1).

As  $D_{\mu\nu}(0)$ ,  $\Gamma_{\mu\nu}^0$  and  $\epsilon_{\alpha\beta}^{\infty}$  are real quantities, by substituting Eqs. (21), (22) and (23) into Eq. (1) we obtain

$$\epsilon_{\alpha\beta}^{\text{AS}}(\omega) = \epsilon_{\alpha\beta}^{\text{AS},\infty} + \frac{2\pi}{V_0} \sum_{\mu\nu} Z_{\mu\alpha}^* \left\{ [D(0) + \bar{\Pi}(\omega) - \omega^2 - i\omega\Gamma^0]^{-1} - [D(0) + \bar{\Pi}^*(\omega) - \omega^2 - i\omega\Gamma^0]^{-1} \right\} Z_{\nu\beta}^*. \quad (24)$$

For  $\omega \ll \Delta$ , the electronic dielectric tensor  $\epsilon_{\alpha\beta}^{\infty}$  is Hermitian (non-dissipative); thus its real part is symmetric and its imaginary part is antisymmetric. The reality condition  $[\epsilon_{\alpha\beta}^{\infty}(\omega)]^* = \epsilon_{\alpha\beta}^{\infty}(-\omega)$  implies that the imaginary-antisymmetric part is odd in frequency, and therefore it vanishes for  $\omega \ll \Delta$ . Hence,  $\text{Im} \epsilon_{\alpha\beta}^{\text{AS},\infty}$  is negligible in the

infrared regime, and can be safely dropped. In the adiabatic approximation, as  $\bar{\Pi}(0) = 0$ , it follows that  $\epsilon_{\alpha\beta}^{\text{AS}} = 0$  when the system is insulating. We complete this theoretical part by noting that the real (dissipative dichroic) and imaginary (reactive dichroic) parts are, respectively, given by:

$$\begin{aligned} \text{Re} \epsilon_{\alpha\beta}^{\text{AS}}(\omega) &= \text{Re} \epsilon_{\alpha\beta}^{\text{AS},\infty} + \frac{\pi}{V_0} \sum_{\mu\nu} Z_{\alpha\mu}^* \left\{ [D(0) + \bar{\Pi}(\omega) - \omega^2 - i\omega\Gamma^0]^{-1} - [D(0) + \bar{\Pi}^*(\omega) - \omega^2 - i\omega\Gamma^0]^{-1} \right\} Z_{\beta\nu}^* \\ &\quad + \frac{\pi}{V_0} \sum_{\mu\nu} Z_{\alpha\mu}^* \left\{ [D(0) + \bar{\Pi}^*(\omega) - \omega^2 + i\omega\Gamma^0]^{-1} - [D(0) + \bar{\Pi}(\omega) - \omega^2 + i\omega\Gamma^0]^{-1} \right\} Z_{\beta\nu}^* \end{aligned} \quad (25)$$

$$\begin{aligned} \text{Im} \epsilon_{\alpha\beta}^{\text{AS}}(\omega) &= \frac{\pi}{V_0} \sum_{\mu\nu} Z_{\alpha\mu}^* \left\{ [D(0) + \bar{\Pi}(\omega) - \omega^2 - i\omega\Gamma^0]^{-1} - [D(0) + \bar{\Pi}^*(\omega) - \omega^2 - i\omega\Gamma^0]^{-1} \right\} Z_{\beta\nu}^* \\ &\quad + \frac{\pi}{V_0} \sum_{\mu\nu} Z_{\alpha\mu}^* \left\{ [D(0) + \bar{\Pi}^*(\omega) - \omega^2 + i\omega\Gamma^0]^{-1} - [D(0) + \bar{\Pi}(\omega) - \omega^2 + i\omega\Gamma^0]^{-1} \right\} Z_{\beta\nu}^*, \end{aligned} \quad (26)$$

where again  $\omega \ll \Delta$  is assumed.

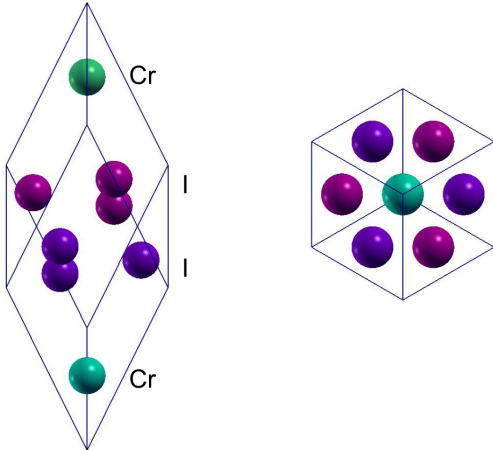
### III. TECHNICAL DETAILS

We simulate the structural, electronic and vibrational properties of  $\text{CrI}_3$  by using the QUANTUM ESPRESSO (QE) code [20]. We adopt the PBE exchange and correlation functional [21]. We use ONCV [22] fully relativistic norm-conserving pseudopotentials for Cr and I from the PseudoDojo [23] repository, option accuracy stringent.  $\text{CrI}_3$  crystallizes in the space group  $R\bar{3}$  (see Fig. 1). We use the experimental lattice parameters  $\approx 7.70\text{\AA}$  and the rhombohedral angle  $\cos(\theta) \approx 0.6025$  ( $\theta \approx 52.93^\circ$ ) and we perform structural optimization of internal coordinates. In the geometrical optimization of the internal coordinates we use a  $4 \times 4 \times 4$  electron momentum mesh and a Fermi-Dirac smearing of  $3 \times 10^{-4}$  Ryd. We use a 120 Ry

cutoff on the kinetic energy and a 4 times larger cutoff for the charge density.

The adiabatic phonon frequencies and the Born effective charge tensor were calculated by using density functional perturbation theory (DFPT) [24]. For technical reasons, the dielectric tensor  $\epsilon_{\alpha\beta}^{\infty}$  and Born effective charge tensor  $Z_{a\alpha\beta}^*$  were calculated in the collinear spin approximation, while the adiabatic phonon frequencies were obtained via a fully relativistic noncollinear DFPT calculation. We do not expect substantial qualitative differences with respect to the case in which the Born effective charges are calculated in the noncollinear fully relativistic case. The calculated  $\epsilon_{\alpha\beta}^{\infty}$  tensors are reported in Tabs. I.

In this work we focus on the infrared active  $E_u$  mode at  $216.4 \text{ cm}^{-1}$ , in the static harmonic approximation. This mode is twofold degenerate in the adiabatic relativistic noncollinear magnetic case.

FIG. 1. Crystal structure of  $\text{CrI}_3$ .

The nonadiabatic dynamical matrix  $D_{a\alpha,b\beta}(\omega)$  was obtained via Eq. 22 using the method developed in Ref. [12] and in the fully relativistic approach by using a  $8 \times 8 \times 8$  electron-momentum grid. The nonadiabatic effects red-shift and induce a  $0.22 \text{ cm}^{-1}$  splitting between the two  $E_u$  modes, which frequencies become  $214.70 \text{ cm}^{-1}$  and  $214.92$ , respectively.

$\epsilon_{\alpha\beta}^\infty$	$\beta = x$	$\beta = y$	$\beta = z$
$\alpha = x$	7.97	0.0	0.0
$\alpha = y$	0.0	7.97	0.0
$\alpha = z$	0.0	0.0	6.07

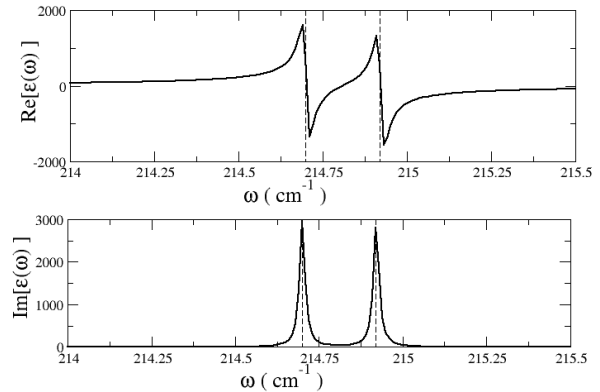
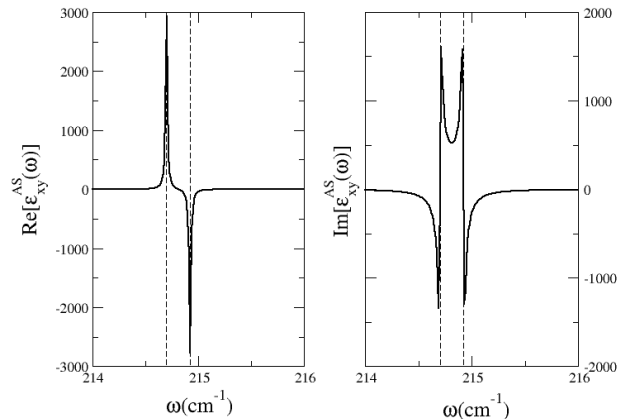
TABLE I. Dielectric tensor  $\epsilon_{\alpha\beta}^\infty$  calculated in density functional perturbation theory in the collinear spin approximation.

## IV. RESULTS

### A. Dielectric function of $\text{CrI}_3$

The calculated real and imaginary parts of the average of the in-plane components of the dielectric function, i.e.  $\epsilon(\omega) = \frac{1}{2}[\epsilon_{xx}(\omega) + \epsilon_{yy}(\omega)]$ , are shown in Fig. 2. The imaginary part peaks at the phonon frequencies splitted by dynamical effects (vertical dashed lines). The splitting between the phonon frequencies induced by the occurrence of phonon chirality is  $\approx 0.22 \text{ cm}^{-1}$ . Nevertheless, the phonon angular momentum associated with each mode is not small, as we evaluate it to be  $\approx \pm\hbar/2$ , in agreement with what reported in [25]. Thus, even for large phonon angular momenta, the induced splitting can be quite small, as already shown in Ref. [12].

The splitting measured in experiments, however, strongly depends on the energy difference occurring between the infrared phonon frequencies and the magnon excitation. In our formalism, as we have neglected the

FIG. 2. Real and imaginary part of  $\epsilon(\omega) = \frac{1}{2}[\epsilon_{xx}(\omega) + \epsilon_{yy}(\omega)]$ . The curves have been broadened with a width of  $0.02 \text{ cm}^{-1}$ . The vertical dashed lines label the phonon frequencies split by the dynamical effects.FIG. 3. Real and imaginary part of  $\epsilon_{xy}^{AS}(\omega) = (\epsilon_{xy}(\omega) - \epsilon_{yx}(\omega))/2$ . The curves have been broadened with a width of  $0.02 \text{ cm}^{-1}$ . The dashed lines mark the phonon frequencies splitted by dynamical effects.

$\omega$ -dependence of the electron-phonon vertex (we use TDDFT with a static electron-phonon vertex), the splitting is the one at frozen magnetic moments, which is necessarily different from the experimental one.

The dissipative (real part) and reactive (imaginary part) dichroic of the dielectric tensor  $\epsilon_{xy}^{AS}(\omega)$  are shown in Fig. 3. Both parts display marked resonances at the position of the two splitted infrared phonon frequencies. We recall that in the absence of chirality or dynamical effects, i.e.  $\bar{\Pi}(\omega) = 0$ , both the real and imaginary parts of  $\epsilon_{xy}^{AS}(\omega)$  would be zero.

## B. Refractive index

We consider light impinging on a sample. We assume the fields to be polarized within the  $xy$  plane and propagating along the  $z$  direction,  $\mathbf{E}e^{i(kz-\omega t)}$  and  $\mathbf{H}e^{i(kz-\omega t)}$ . We define the refractive index as  $n = ck/\omega$ . The fields inside the material satisfy the following relations:

$$\mathbf{H} = n\hat{\mathbf{z}} \times \mathbf{E} \quad (27)$$

and

$$\mathbf{D} = \varepsilon\mathbf{E} = -n\hat{\mathbf{z}} \times \mathbf{H}. \quad (28)$$

In vacuum,  $n = 1$ . if we combine  $\mathbf{D} = -\mathbf{n} \times \mathbf{H}$  with  $\mathbf{n} = n\hat{\mathbf{z}}$  and  $\mathbf{H} = \mathbf{n} \times \mathbf{E}$ , we arrive at

$$\mathbf{D} = n^2 \mathbf{E} - (\mathbf{n} \cdot \mathbf{E}) \mathbf{n}, \quad (29)$$

which can be written as

$$\begin{aligned} D_x &= n^2 E_x = n^2 (\varepsilon_{xx}^{-1} D_x + \varepsilon_{xy}^{-1} D_y) \\ D_y &= n^2 E_y = n^2 (\varepsilon_{yx}^{-1} D_x + \varepsilon_{yy}^{-1} D_y) \\ D_z &= 0. \end{aligned} \quad (30)$$

or, in matrix form,

$$\begin{pmatrix} \varepsilon_{xx}^{-1} - n_a^{-2} & \varepsilon_{xy}^{-1} \\ \varepsilon_{yx}^{-1} & \varepsilon_{yy}^{-1} - n_a^{-2} \end{pmatrix} \begin{pmatrix} D_{a,x} \\ D_{a,y} \end{pmatrix} = \begin{pmatrix} 0 \\ 0 \end{pmatrix}. \quad (31)$$

which is an eigenvalue problem of a complex and non-Hermitian  $2 \times 2$  matrix. We label the eigenvectors and the corresponding eigenvalues as  $\mathbf{D}_a = \varepsilon\mathbf{E}_a$  and  $n_a^{-2}$ , respectively ( $a = 1, 2$ ). Both eigenvalues and eigenvectors are complex.

Therefore,

$$n_a^{-2} = \frac{\varepsilon_{xx}^{-1} + \varepsilon_{yy}^{-1}}{2} \pm \sqrt{\left(\frac{\varepsilon_{xx}^{-1} - \varepsilon_{yy}^{-1}}{2}\right)^2 + \varepsilon_{xy}^{-1} \varepsilon_{yx}^{-1}}, \quad (32)$$

There are two possible values for each refractive index  $n_a(\omega)$ , as  $n_a(\omega) = \pm 1/\sqrt{n_a^{-2}(\omega)}$ . Assuming that the vacuum is in  $z < 0$  and the material is in  $z > 0$ ,  $n_a$  must satisfy both  $\text{Re } n_a > 0$  (propagating along the  $+z$  direction in the material) and  $\text{Im } n_a > 0$  (decaying in the material).

The eigenvalue  $n_a^{-2}$  satisfies the causality relation, that is, the imaginary part of  $n_a^{-2}$  is negative to make the imaginary part of  $n_a^2$  positive. In order to demonstrate this point, we assume that the  $3 \times 3$  dielectric function is written as a sum of two terms,  $\varepsilon = \varepsilon_1 + i\varepsilon_2$ , where  $\varepsilon_1$  and  $\varepsilon_2$  are both hermitian. Then, for arbitrary  $\mathbf{E}$  and  $\mathbf{D}$  vectors satisfying  $\mathbf{D} = \varepsilon\mathbf{E}$ , we have  $\mathbf{D}^\dagger \varepsilon^{-1} \mathbf{D} = \mathbf{E}^\dagger \varepsilon^\dagger \mathbf{E} = \mathbf{E}^\dagger (\varepsilon_1 - i\varepsilon_2) \mathbf{E}$ . Because  $\varepsilon_2$  is positive-definite,

$$\text{Im } \mathbf{D}^\dagger \varepsilon^{-1} \mathbf{D} = \mathbf{E}^\dagger (-\varepsilon_2) \mathbf{E} < 0 \quad (33)$$

always. Now, if we choose  $\mathbf{D}$  to be an eigenvector satisfying Eqs. (30) and (31),

$$\mathbf{D}_a^\dagger \varepsilon^{-1} \mathbf{D}_a = n_a^{-2} \mathbf{D}_a^\dagger \mathbf{D}_a. \quad (34)$$

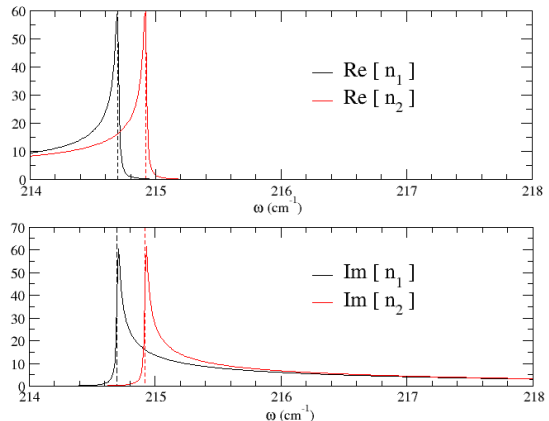


FIG. 4. Real and imaginary parts of the refractive index  $n(\omega)$ . The vertical dashed lines marks the energy of the infrared phonons split by dynamical effects.

Plugging Eq. (34) into Eq. (33), we arrive at  $\text{Im } n_a^{-2} < 0$ , completing the proof. This condition is equivalent to stating that the imaginary part of the eigenvalues of  $\varepsilon$  is positive.

The calculated real and imaginary parts of the dynamical refraction index  $n_a(\omega)$  are shown in Fig. 4. In Fig. 4 we choose the solution of the equation  $n_a(\omega) = \pm 1/\sqrt{n_a^{-2}(\omega)}$  respecting the dissipative character of  $n_a(\omega)$  inside the material (i.e. with  $\text{Im } n_a(\omega) > 0$ ). As it can be seen, left and right polarized light experience two different refraction indexes that will generate a nonzero circular dichroic absorption as well as nonzero Faraday and Kerr rotations.

## C. Reflection from an infinitely thick sample

In this section we obtain the equations for the reflectivity and the circular dichroic absorption from a measurement in reflection from a sample assumed to have an infinite thickness.

We define the left and right polarization as  $\hat{\mathbf{e}}_{\pm 1} = \frac{\hat{\mathbf{x}} \pm i\hat{\mathbf{y}}}{\sqrt{2}}$ , where  $\hat{\mathbf{x}}$  and  $\hat{\mathbf{y}}$  are the orthogonal unit vectors in the  $xy$ -plane. We define the incident, reflected, and transmitted waves for circularly polarized incidence (with handedness  $s = \pm 1$ ) as follows:

$$\begin{aligned} \mathbf{E}_{i,s} &= \hat{\mathbf{e}}_s e^{i\omega z/c} e^{-i\omega t} \\ \mathbf{E}_{r,s} &= (\hat{\mathbf{e}}_{+1} r_{+1,s} + \hat{\mathbf{e}}_{-1} r_{-1,s}) e^{-i\omega z/c} e^{-i\omega t} \\ \mathbf{E}_{t,s} &= \mathbf{E}_1 t_{1,s} e^{i\omega n_1 z/c} + \mathbf{E}_2 t_{2,s} e^{i\omega n_2 z/c} e^{-i\omega t}. \end{aligned} \quad (35)$$

The incident, reflected and transmitted magnetic fields can be obtained from  $\mathbf{H} = -i\frac{c}{\omega} \nabla \times \mathbf{E}$ .

The coefficients  $r_{+1,s}$ ,  $r_{-1,s}$ ,  $t_{1,s}$ , and  $t_{2,s}$  are determined from the conditions that the tangential ( $xy$ ) com-

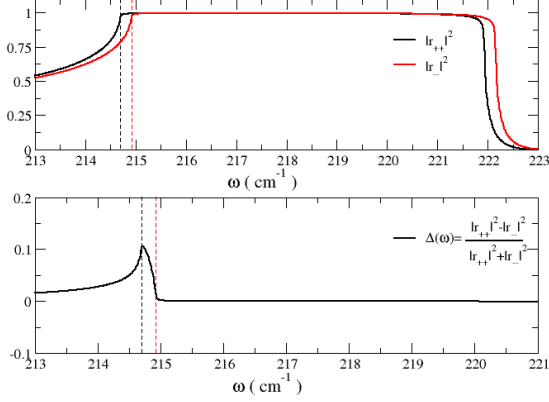


FIG. 5. Reflectivity (top) and Dichroic absorption (bottom) in  $\text{CrI}_3$  in the assumption of a measurement in reflection from an infinite sample. The vertical dashed lines marks the energy of the infrared phonons split by dynamical effects.

ponents of the fields  $\mathbf{E}$  and  $\mathbf{H}$  are continuous across the boundary, namely:

$$\begin{aligned} \hat{\mathbf{e}}_s + \hat{\mathbf{e}}_{+1} r_{+1,s} + \hat{\mathbf{e}}_{-1} r_{-1,s} &= \mathbf{E}_1 t_{1,s} + \mathbf{E}_2 t_{2,s} \\ \hat{\mathbf{e}}_s - \hat{\mathbf{e}}_{+1} r_{+1,s} - \hat{\mathbf{e}}_{-1} r_{-1,s} &= n_1 \mathbf{E}_1 t_{1,s} + n_2 \mathbf{E}_2 t_{2,s}, \end{aligned} \quad (36)$$

From the solution of this 8 dimensional linear system we determine all the necessary coefficients. We underline that  $t_{1,s}$  and  $t_{2,s}$  do depend on the magnitudes of  $\mathbf{E}_1$  and  $\mathbf{E}_2$ , respectively; however, their products  $t_{1,s} \mathbf{E}_1$  and  $t_{2,s} \mathbf{E}_2$  do not.

The reflectivities for two different circular polarizations are  $|r_{+,+}|^2$  and  $|r_{-,-}|^2$  and they are plotted in the top panel of Fig. 5. The calculated reflectivity agrees qualitatively and semiquantitatively with experiments [26, 27].

The dichroic absorption signal is then

$$\Delta(\omega) = \frac{|r_{+,+}|^2 - |r_{-,-}|^2}{|r_{+,+}|^2 + |r_{-,-}|^2} \quad (37)$$

The result of Eq. 37 is shown in Fig. 5. As it can be seen, even if the splitting is very small as the adiabatic local density approximation employed in the calculation, the circular dichroic absorption is sizable and can be measured.

#### D. Kerr rotation from the reflection of an infinite thick sample

Kerr rotation is the rotation of the polarization of light when light is reflected from a magnetic material or in the presence of an external magnetic field. In order to model this effect, we assume that the incident light has

polarization  $\hat{\mathbf{e}}_\theta = \hat{\mathbf{x}} \cos \theta + \hat{\mathbf{y}} \sin \theta$ . Then, electric fields can be written as

$$\begin{aligned} \mathbf{E}_{i,\theta} &= \hat{\mathbf{e}}_\theta e^{i\omega z/c} e^{-i\omega t} \\ \mathbf{E}_{r,\theta} &= (\hat{\mathbf{x}} r_{x,\theta} + \hat{\mathbf{y}} r_{y,\theta}) e^{-i\omega z/c} e^{-i\omega t} \\ \mathbf{E}_{t,\theta} &= \mathbf{E}_1 t_{1,\theta} e^{i\omega n_1 z/c} + \mathbf{E}_2 t_{2,\theta} e^{i\omega n_2 z/c} e^{-i\omega t}. \end{aligned} \quad (38)$$

Using the same boundary conditions as in the case of the circular polarization, we arrive at

$$\begin{aligned} \hat{\mathbf{e}}_\theta + \hat{\mathbf{x}} r_{x,\theta} + \hat{\mathbf{y}} r_{y,\theta} &= \mathbf{E}_1 t_{1,\theta} + \mathbf{E}_2 t_{2,\theta} \\ \hat{\mathbf{e}}_\theta - \hat{\mathbf{x}} r_{x,\theta} - \hat{\mathbf{y}} r_{y,\theta} &= n_1 \mathbf{E}_1 t_{1,\theta} + n_2 \mathbf{E}_2 t_{2,\theta}, \end{aligned} \quad (39)$$

The solution of this 4-dimensional linear system leads to  $r_{x,\theta}$ ,  $r_{y,\theta}$ ,  $t_{1,\theta}$ , and  $t_{2,\theta}$ .

The angle of the polarization and the ellipticity can be obtained directly from these parameters as follows. We define the three Stokes parameters  $s_1$ ,  $s_2$  and  $s_3$  as

$$\begin{aligned} s_1 &= I_{0^\circ} - I_{90^\circ} = |r_{x,\theta}|^2 - |r_{y,\theta}|^2 \\ s_2 &= I_{+45^\circ} - I_{-45^\circ} = \left| \frac{r_{x,\theta} + r_{y,\theta}}{\sqrt{2}} \right|^2 - \left| \frac{r_{x,\theta} - r_{y,\theta}}{\sqrt{2}} \right|^2 \\ s_3 &= I_{\text{RCP}} - I_{\text{LCP}} = \left| \frac{r_{x,\theta} + i r_{y,\theta}}{\sqrt{2}} \right|^2 - \left| \frac{r_{x,\theta} - i r_{y,\theta}}{\sqrt{2}} \right|^2, \end{aligned} \quad (40)$$

where we have used the polarizations for RCP and LCP are  $\hat{\mathbf{e}}_{\text{RCP}} = \hat{\mathbf{e}}_{-1} = \frac{\hat{\mathbf{x}} - i\hat{\mathbf{y}}}{\sqrt{2}}$  and  $\hat{\mathbf{e}}_{\text{LCP}} = \hat{\mathbf{e}}_{+1} = \frac{\hat{\mathbf{x}} + i\hat{\mathbf{y}}}{\sqrt{2}}$ , respectively.

Then, the polarization angle is given by

$$\psi = \frac{1}{2} \tan^{-1} \frac{s_2}{s_1}. \quad (41)$$

and the ellipticity can be obtained from

$$\frac{b}{a} = \tan \left( \frac{1}{2} \tan^{-1} \frac{s_3}{\sqrt{s_1^2 + s_2^2}} \right), \quad (42)$$

where  $a$  and  $b$  are the major and minor axes of an ellipse. The solution of the linear system is shown in Fig. 6 for  $\theta = 0^\circ$ .

#### E. Dichroism of light transmitted through a slab of thickness $d$

As done in the previous sections, we write down the fields inside a sample of finite thickness  $d$  in a point  $0 < z < d$ . We neglect multiple reflection and consider 4 electric fields, namely the incident  $\mathbf{E}_{i,s}$ , the reflected  $\mathbf{E}_{r,s}$ , the transmitted  $\mathbf{E}_{t,s}$  and the field inside the medium  $\mathbf{E}_{m,s}$ . For the incident, reflected, intermediate

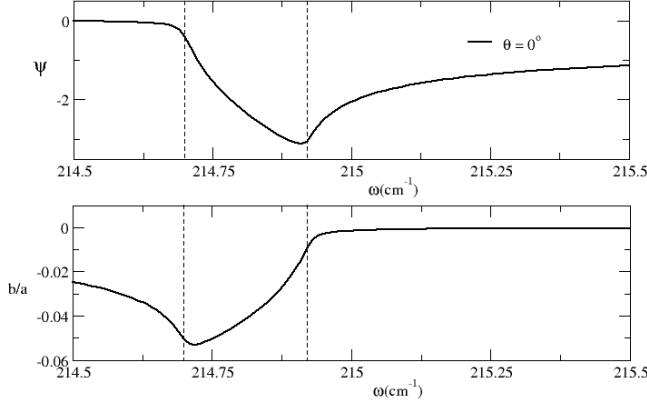


FIG. 6. Polarization angle (top) and ellipticity (bottom) for Kerr rotation as obtained from the reflection from an infinite thick sample of  $\text{CrI}_3$  for  $\theta = 0^\circ$ . The vertical dashed lines mark the energy of the infrared phonons split by dynamical effects.

( $0 < z < d$ ), and transmitted fields we have :

$$\begin{aligned}
 \mathbf{E}_{i,s} &= \hat{\mathbf{e}}_s e^{i\omega z/c} e^{-i\omega t} \\
 \mathbf{E}_{r,s} &= (\hat{\mathbf{e}}_{+1} r_{+1,s} + \hat{\mathbf{e}}_{-1} r_{-1,s}) e^{-i\omega z/c} e^{-i\omega t} \\
 \mathbf{E}_{m,s} &= \mathbf{E}_1 \left( m_{11,s} e^{i\omega n_1 z/c} + m_{12,s} e^{-i\omega n_1 z/c} \right) e^{-i\omega t} \\
 &\quad + \mathbf{E}_2 \left( m_{21,s} e^{i\omega n_2 z/c} + m_{22,s} e^{-i\omega n_2 z/c} \right) e^{-i\omega t} \\
 \mathbf{E}_{t,s} &= (\hat{\mathbf{e}}_{+1} t_{+1,s} + \hat{\mathbf{e}}_{-1} t_{-1,s}) e^{i\omega z/c} e^{-i\omega t}. \quad (43)
 \end{aligned}$$

The boundary conditions at  $z = 0$  and  $z = d$  give

$$\begin{aligned}
 &\hat{\mathbf{e}}_s + \hat{\mathbf{e}}_{+1} r_{+1,s} + \hat{\mathbf{e}}_{-1} r_{-1,s} \\
 &= \mathbf{E}_1 (m_{11,s} + m_{12,s}) + \mathbf{E}_2 (m_{21,s} + m_{22,s}), \\
 &\hat{\mathbf{e}}_s - \hat{\mathbf{e}}_{+1} r_{+1,s} - \hat{\mathbf{e}}_{-1} r_{-1,s} \\
 &= n_1 \mathbf{E}_1 (m_{11,s} - m_{12,s}) + n_2 \mathbf{E}_2 (m_{21,s} - m_{22,s}) \quad (44)
 \end{aligned}$$

and

$$\begin{aligned}
 &\mathbf{E}_1 \left( m_{11,s} e^{i\omega n_1 d/c} + m_{12,s} e^{-i\omega n_1 d/c} \right) \\
 &+ \mathbf{E}_2 \left( m_{21,s} e^{i\omega n_2 d/c} + m_{22,s} e^{-i\omega n_2 d/c} \right) \\
 &= (\hat{\mathbf{e}}_{+1} t_{+1,s} + \hat{\mathbf{e}}_{-1} t_{-1,s}) e^{i\omega d/c}, \\
 &n_1 \mathbf{E}_1 \left( m_{11,s} e^{i\omega n_1 d/c} - m_{12,s} e^{-i\omega n_1 d/c} \right) \\
 &+ n_2 \mathbf{E}_2 \left( m_{21,s} e^{i\omega n_2 d/c} - m_{22,s} e^{-i\omega n_2 d/c} \right) \\
 &= (\hat{\mathbf{e}}_{+1} t_{+1,s} + \hat{\mathbf{e}}_{-1} t_{-1,s}) e^{i\omega d/c}, \quad (45)
 \end{aligned}$$

respectively. We now have eight unknowns,  $r_{+1,s}$ ,  $r_{-1,s}$ ,  $m_{11,s}$ ,  $m_{12,s}$ ,  $m_{21,s}$ ,  $m_{22,s}$ ,  $t_{+1,s}$ , and  $t_{-1,s}$ , and eight

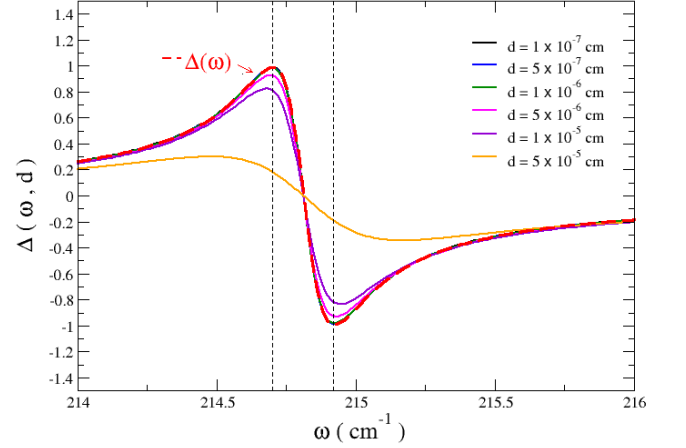


FIG. 7. Dichroic absorption in  $\text{CrI}_3$  in the assumption of a measurement in transmission from a sample of thickness  $d$ . The red continuous line is obtained from Eq. 47. The vertical dashed lines mark the energy of the infrared phonons splitted by dynamical effects.

equations [Eqs. (44) and (45)]. The circular dichroism for absorbance (neglecting internal reflections) is obtained as:

$$\Delta(\omega, d) = \frac{(1 - |t_{+1,+1}|^2) - (1 - |t_{-1,-1}|^2)}{(1 - |t_{+1,+1}|^2) + (1 - |t_{-1,-1}|^2)}, \quad (46)$$

The dichroism in absorbance depends, obviously, on the thickness of the material. In the usual experimental assumption is that the sample is thin and that  $\Delta(\omega, d)$  does not depend on  $d$ . As can be seen from Fig. 7,  $\Delta(\omega, d)$  is weakly dependent on  $d$  in the region where the two phonon resonances occur ( $214.5 < \omega < 215.25$ ) only for  $d \leq 10^{-6}$  cm. We note that in this region the position of the minimum and maximum in the circular dichroic absorption are located at the energies of phonon frequencies split by dynamical effects. For thicker samples, the signal is progressively suppressed, and the minimum and maximum do not correspond anymore with the energies of the phonon frequencies.

The limit of thickness going to zero in Eq. 46 leads to the expression

$$\Delta(\omega) = \frac{\text{Re}(\varepsilon_{xy} - \varepsilon_{yx})}{\text{Im}(\varepsilon_{xx} + \varepsilon_{yy})}. \quad (47)$$

that is also plotted in Fig. 7 and matches very well the smallest sample thicknesses.

## F. Faraday rotation

In this section, for completeness, we obtain the equation for Faraday rotation, i.e. the rotation of the polar-

ization of light when light is transmitted through a magnetic material or in the presence of an external magnetic field.

We consider a linear polarized incident light. The equations for the electric fields are:

$$\begin{aligned}
\mathbf{E}_{i,\theta} &= \hat{\mathbf{e}}_\theta e^{i\omega z/c} e^{-i\omega t} \\
\mathbf{E}_{r,\theta} &= (\hat{\mathbf{e}}_x r_{x,s} + \hat{\mathbf{e}}_y r_{y,s}) e^{-i\omega z/c} e^{-i\omega t} \\
\mathbf{E}_{m,\theta} &= \mathbf{E}_1 \left( m_{11,\theta} e^{i\omega n_1 z/c} + m_{12,\theta} e^{-i\omega n_1 z/c} \right) e^{-i\omega t} \\
&\quad + \mathbf{E}_2 \left( m_{21,\theta} e^{i\omega n_2 z/c} + m_{22,\theta} e^{-i\omega n_2 z/c} \right) e^{-i\omega t} \\
\mathbf{E}_{t,\theta} &= (\hat{\mathbf{e}}_x t_{x,\theta} + \hat{\mathbf{e}}_y t_{y,\theta}) e^{i\omega z/c} e^{-i\omega t} \quad (48)
\end{aligned}$$

The boundary conditions at  $z = 0$  and  $z = d$  give

$$\begin{aligned}
&\hat{\mathbf{e}}_\theta + \hat{\mathbf{e}}_x r_{x,\theta} + \hat{\mathbf{e}}_y r_{y,\theta} \\
&= \mathbf{E}_1 (m_{11,\theta} + m_{12,\theta}) + \mathbf{E}_2 (m_{21,\theta} + m_{22,\theta}), \\
&\hat{\mathbf{e}}_\theta - \hat{\mathbf{e}}_x r_{x,\theta} - \hat{\mathbf{e}}_y r_{y,\theta} \\
&= n_1 \mathbf{E}_1 (m_{11,\theta} - m_{12,\theta}) + n_2 \mathbf{E}_2 (m_{21,\theta} - m_{22,\theta}) \quad (49)
\end{aligned}$$

and

$$\begin{aligned}
&\mathbf{E}_1 \left( m_{11,\theta} e^{i\omega n_1 d/c} + m_{12,\theta} e^{-i\omega n_1 d/c} \right) \\
&+ \mathbf{E}_2 \left( m_{21,\theta} e^{i\omega n_2 d/c} + m_{22,\theta} e^{-i\omega n_2 d/c} \right) \\
&= (\hat{\mathbf{e}}_x t_{x,\theta} + \hat{\mathbf{e}}_y t_{y,\theta}) e^{i\omega d/c}, \\
&n_1 \mathbf{E}_1 \left( m_{11,\theta} e^{i\omega n_1 d/c} - m_{12,\theta} e^{-i\omega n_1 d/c} \right) \\
&+ n_2 \mathbf{E}_2 \left( m_{21,\theta} e^{i\omega n_2 d/c} - m_{22,\theta} e^{-i\omega n_2 d/c} \right) \\
&= (\hat{\mathbf{e}}_x t_{x,\theta} + \hat{\mathbf{e}}_y t_{y,\theta}) e^{i\omega d/c}, \quad (50)
\end{aligned}$$

respectively. We now have eight unknowns,  $r_{x,\theta}$ ,  $r_{y,\theta}$ ,  $m_{11,\theta}$ ,  $m_{12,\theta}$ ,  $m_{21,\theta}$ ,  $m_{22,\theta}$ ,  $t_{x,\theta}$ , and  $t_{y,\theta}$ , and eight equations [Eqs. (49) and (50)].

The polarization angle and the ellipticity for transmitted light can be obtained using Eqs. (40), (41), and (42), except that now  $t_{x,\theta}$  and  $t_{y,\theta}$  must be used at places of  $r_{x,\theta}$  and  $r_{y,\theta}$ , respectively.

### G. Effect of a large drag-force coefficient.

In the calculations of the magneto-optical effects carried out in the previous sections, we consider a drag force coefficient  $\tilde{\Gamma} = 0.02 \text{ cm}^{-1}$  corresponding to the case of  $\tilde{\Gamma} \ll \Delta\omega = 0.22 \text{ cm}^{-1}$ , where  $\Delta\omega$  is the non-adiabatic phonon splitting calculated within time dependent density functional theory in the adiabatic local-density approximation. This approximation assumes, however, adiabatic separation between the ionic and spin dynamics and can result in incorrect values of the non-adiabatic phonon splitting. Thus, in the experimental situation, the phonon splitting could even be smaller than  $\tilde{\Gamma}$ . It is then important to verify how the calculated spectra depends on the ratio  $\tilde{\Gamma}/\Delta\omega$  to verify that the circular

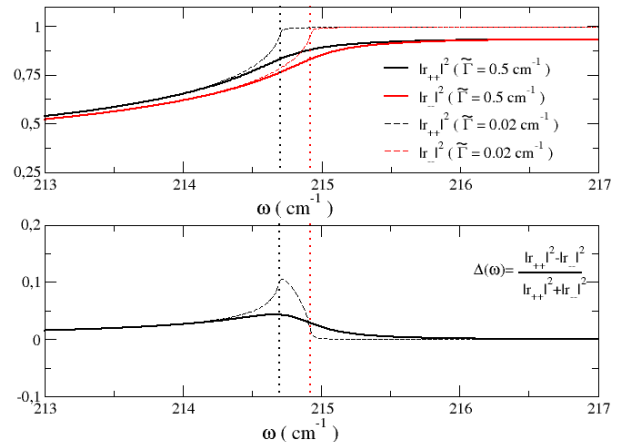


FIG. 8. Reflectivity (top) and Dichroic absorption (bottom) in CrI<sub>3</sub> in the assumption of a measurement in reflection from an infinite sample and for two different values of the drag force coefficient. The vertical dotted lines mark the energy of the infrared frequencies split by dynamical effects.

dichroic signal remains visible even under this condition.

In Fig. 8 we plot the left and right reflectivities in reflection from an infinite sample and for a drag force coefficient that is larger than twice the splitting of the phonon modes. As can be seen in the bottom panel, the circular dichroic signal is still clearly visible.

The same occurs for the circular dichroism in transmission (see Fig. 9). The larger force drag coefficient reduces the amplitude of the  $\Delta(\omega, d)$  signal that, even in this case, remains detectable. However, for large  $\tilde{\Gamma}$ , the minimum and maximum of the circular dichroic signal do not measure directly the energy of the split infrared phonon frequencies.

## V. CONCLUSIONS

Probing phonon chirality in solids is not easy as the the phonon spectrum splitting induced by non-adiabatic effects are generally small despite the value of the phonon angular momentum comparable to the spin one[5].

In our work, we have shown that a reliable probe of phonon chirality is the measurement of circular-dichroic infrared absorption. Indeed, a finite circular dichroic infrared absorption arises solely from dynamical effects and it is exactly zero in the static case.

We obtain the equations for the optical absorption and the Faraday and Kerr effects. We applied our derivation to the case of CrI<sub>3</sub> and have shown that the circular dichroic absorption is non-negligible and sizeable, both in reflection and in transition.

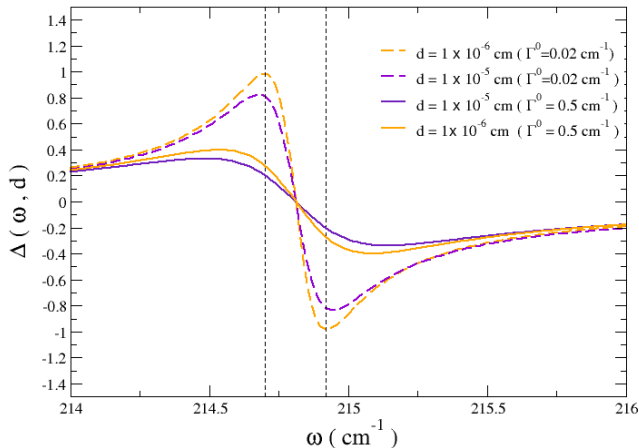


FIG. 9. Dichroic absorption in  $\text{CrI}_3$  in the assumption of a measurement in transmission from a sample of thickness  $d$  as a function of the force drag coefficient  $\bar{\Gamma}$ . The vertical dashed lines mark the energy of the infrared phonons split by dynamical effects.

Finally, we point out that although our calculation suffers from the neglecting of the resonance with the magnon modes, resulting in an incorrect phonon splitting, we be-

lieve it to be quite reliable and significant for what concerns the intensity of the circular dichroic signal. What we expect is mostly a change in the magnitude of the splitting of the infrared active phonons, that in our case is probably too small.

*Note added:* In the final stages of this work, we became aware of a preprint [28] calculating the infrared circular dichroic absorption both with frozen spins (similar to the present work), and with relaxed spins (including the resonance with the magnons). In the frozen-spin case, the authors find qualitatively similar results to ours. Moreover, they obtain a strong enhancement of the circular dichroic signal when spin-canting is allowed, confirming the importance of the effect.

## ACKNOWLEDGMENTS

We acknowledge the useful discussions with O. Bistoni, M. Furci, P. Giannozzi and M. Stengel. C.-H.P. was supported by the Korean NRF No-2023R1A2C1007297. I. S. was supported by Grant No. PID2021-129035NB-I00 funded by MCIN/AEI/10.13039/501100011033 and by ERDF/EU. M.C was funded by the European Union (ERC, DELIGHT, 101052708). Views and opinions expressed are however those of the author(s) only and do not necessarily reflect those of the European Union or the European Research Council. Neither the European Union nor the granting authority can be held responsible for them.

- 
- [1] C. Strohm, G. L. J. A. Rikken, and P. Wyder, Phenomenological evidence for the phonon hall effect, *Phys. Rev. Lett.* **95**, 155901 (2005).
- [2] C. A. Mead, The geometric phase in molecular systems, *Rev. Mod. Phys.* **64**, 51 (1992).
- [3] R. Resta, Manifestations of Berry's phase in molecules and condensed matter, *J. Phys.: Condens. Matter* **12**, R107 (2000).
- [4] T. Qin, J. Zhou, and J. Shi, Berry curvature and the phonon hall effect, *Phys. Rev. B* **86**, 104305 (2012).
- [5] L. Zhang and Q. Niu, Angular momentum of phonons and the einstein-de haas effect, *Phys. Rev. Lett.* **112**, 085503 (2014).
- [6] T. Saito, K. Misaki, H. Ishizuka, and N. Nagaosa, Berry phase of phonons and thermal hall effect in nonmagnetic insulators, *Phys. Rev. Lett.* **123**, 255901 (2019).
- [7] D. Saporov, B. Xiong, Y. Ren, and Q. Niu, Lattice dynamics with molecular berry curvature: Chiral optical phonons, *Phys. Rev. B* **105**, 064303 (2022).
- [8] M. Born and K. Huang, *Dynamical Theory of Crystal Lattices* (Oxford University Press, 1954).
- [9] H. Zhu, J. Yi, M.-Y. Li, J. Xiao, L. Zhang, C.-W. Yang, R. A. Kaindl, L.-J. Li, Y. Wang, and X. Zhang, Observation of chiral phonons, *Science* **359**, 579 (2018).
- [10] M. Hamada, E. Minamitani, M. Hirayama, and S. Murakami, Phonon angular momentum induced by the temperature gradient, *Phys. Rev. Lett.* **121**, 175301 (2018).
- [11] C. A. Mead and D. G. Truhlar, On the determination of born-oppenheimer nuclear motion wave functions including complications due to conical intersections and identical nuclei, *The Journal of Chemical Physics* **70**, 2284 (1979), [https://pubs.aip.org/aip/jcp/article-pdf/70/5/2284/18916340/2284\\_1\\_online.pdf](https://pubs.aip.org/aip/jcp/article-pdf/70/5/2284/18916340/2284_1_online.pdf).
- [12] O. Bistoni, F. Mauri, and M. Calandra, Intrinsic vibrational angular momentum from nonadiabatic effects in noncollinear magnetic molecules, *Phys. Rev. Lett.* **126**, 225703 (2021).
- [13] J. Bonini, S. Ren, D. Vanderbilt, M. Stengel, C. E. Dreyer, and S. Coh, Frequency splitting of chiral phonons from broken time-reversal symmetry in  $\text{crI}_3$ , *Phys. Rev. Lett.* **130**, 086701 (2023).
- [14] S. Ren, J. Bonini, M. Stengel, C. E. Dreyer, and D. Vanderbilt, Adiabatic dynamics of coupled spins and phonons in magnetic insulators, *Phys. Rev. X* **14**, 011041 (2024).
- [15] L. Du, J. Tang, Y. Zhao, X. Li, R. Yang, X. Hu, X. Bai, X. Wang, K. Watanabe, T. Taniguchi, D. Shi, G. Yu, X. Bai, T. Hasan, G. Zhang, and Z. Sun, Lattice Dynamics, Phonon Chirality, and Spin-Phonon Coupling in 2D Itinerant Ferromagnet  $\text{Fe}_3\text{GeTe}_2$ , *Advanced Functional Materials* **29**, 1904734 (2019).
- [16] T. Yin, K. A. Ulman, S. Liu, A. Granados del Águila, Y. Huang, L. Zhang, M. Serra, D. Sedmidubsky, Z. Sofer,

- S. Y. Quek, and Q. Xiong, Chiral phonons and giant magneto-optical effect in crbr3 2d magnet, *Advanced Materials* **33**, 2101618 (2021).
- [17] K. Shinagawa, Faraday and Kerr Effects in Ferromagnets, in *Magneto-Optics*, edited by S. Sugano and N. Kojima (Springer, 1989).
- [18] M. Calandra, G. Profeta, and F. Mauri, Adiabatic and nonadiabatic phonon dispersion in a wannier function approach, *Phys. Rev. B* **82**, 165111 (2010).
- [19] X. Gonze and C. Lee, Dynamical matrices, born effective charges, dielectric permittivity tensors, and interatomic force constants from density-functional perturbation theory, *Phys. Rev. B* **55**, 10355 (1997).
- [20] P. Giannozzi, O. Andreussi, T. Brumme, O. Bunau, M. B. Nardelli, M. Calandra, R. Car, C. Cavazzoni, D. Ceresoli, M. Cococcioni, N. Colonna, I. Carnimeo, A. D. Corso, S. de Gironcoli, P. Delugas, R. A. D. Jr, A. Ferretti, A. Floris, G. Fratesi, G. Fugallo, R. Gebauer, U. Gerstmann, F. Giustino, T. Gorni, J. Jia, M. Kawamura, H.-Y. Ko, A. Kokalj, E. Küçükbenli, M. Lazzeri, M. Marsili, N. Marzari, F. Mauri, N. L. Nguyen, H.-V. Nguyen, A. O. de-la Roza, L. Paulatto, S. Poncé, D. Rocca, R. Sabatini, B. Santra, M. Schlipf, A. P. Seitsonen, A. Smogunov, I. Timrov, T. Thonhauser, P. Umari, N. Vast, X. Wu, and S. Baroni, Advanced capabilities for materials modelling with quantum espresso, *Journal of Physics: Condensed Matter* **29**, 465901 (2017).
- [21] J. P. Perdew, K. Burke, and M. Ernzerhof, Generalized gradient approximation made simple [phys. rev. lett. 77, 3865 (1996)], *Phys. Rev. Lett.* **78**, 1396 (1997).
- [22] D. R. Hamann, Optimized norm-conserving vanderbilt pseudopotentials, *Phys. Rev. B* **88**, 085117 (2013).
- [23] M. van Setten, M. Giantomassi, E. Bousquet, M. Verstraete, D. Hamann, X. Gonze, and G.-M. Rignanese, The pseudodojo: Training and grading a 85 element optimized norm-conserving pseudopotential table, *Computer Physics Communications* **226**, 39 (2018).
- [24] S. Baroni, S. de Gironcoli, A. Dal Corso, and P. Giannozzi, Phonons and related crystal properties from density-functional perturbation theory, *Rev. Mod. Phys.* **73**, 515 (2001).
- [25] J. Bonini, S. Ren, D. Vanderbilt, M. Stengel, C. E. Dreyer, and S. Coh, Frequency splitting of chiral phonons from broken time-reversal symmetry in cri<sub>3</sub>, *Phys. Rev. Lett.* **130**, 086701 (2023).
- [26] L. Tomarchio, L. Mosesso, S. Macis, L. T. Nguyen, A. Grilli, M. Romani, M. Cestelli Guidi, R. J. Cava, and S. Lupi, Phonon anharmonicity and spin-phonon coupling in cri<sub>3</sub>, *Materials* **16**, 10.3390/ma16144909 (2023).
- [27] L. Tomarchio, S. Macis, L. Mosesso, L. T. Nguyen, A. Grilli, M. C. Guidi, R. J. Cava, and S. Lupi, Low energy electrodynamics of cri<sub>3</sub> layered ferromagnet, *Scientific Reports* **11**, 23405 (2021).
- [28] M. Royo and M. Stengel, Dynamical response of noncollinear spin systems at constrained magnetic moments, arxiv:2501.10188 <https://doi.org/10.48550/arXiv.2501.10188>.